

# Preparation, Characterization, and Size Control of Chemically Synthesized CdS Nanoparticles Capped with Poly(ethylene glycol)

R. SEOUDI,<sup>1,2</sup> S.H.A. ALLEHYANI,<sup>2</sup> D.A. SAID,<sup>2,3</sup> A.R. LASHIN,<sup>2,4,5</sup>  
and A. ABUELSAYED<sup>1</sup>

1.—Physics Division, Spectroscopy Department, NRC, Dokki, Cairo 12311, Egypt. 2.—Department of Physics, College of Applied Science, Umm Al-Qura University, Makkah 21955, Saudi Arabia. 3.—Physics Department, Faculty of Girls for Art, Sciences and Education, Ain Shams University, Cairo 1175, Egypt. 4.—Department of Physics, Faculty of Science, Mansoura University, Mansoura 35516, Egypt. 5.—e-mail: lashingi@mans.edu.eg

We prepared cadmium sulfide (CdS) nanoparticles of a specific size via chemical precipitation at room temperature and characterized them using high-resolution transmission electron microscopy, x-ray powder diffraction, ultraviolet–visible spectroscopy, and Fourier-transform infrared (FTIR) measurements. The results showed that the samples were grown with a cubic phase; the particle size could be changed from 2 nm to 4 nm by varying the molar ratios of the precursors (cadmium chloride and sodium sulfide) in the presence of poly(ethylene glycol) (PEG) as an effective capping agent. The optical bandgap of the synthesized nanoparticles was calculated and ranged from 2.73 eV to 2.92 eV depending on the particle size. A large blue-shift from the bulk bandgap (2.42 eV) was observed owing to the quantum size effect. Surface passivation and adsorption of PEG on the CdS nanoparticles was explained on the basis of FTIR measurements; two bands were observed at  $476\text{ cm}^{-1}$  and  $622\text{ cm}^{-1}$ , corresponding to cadmium and sulfide stretching vibrations. We conclude that particle size can be controlled by varying the molar ratios of the precursors. Owing to the PEG encapsulation, the as-prepared samples were extremely stable over time.

**Key words:** Cadmium sulfide nanoparticles, poly(ethylene glycol), HR-TEM, XRD, UV–Vis

## INTRODUCTION

In recent years, nanostructured semiconductor materials with dimension of less than 100 nm have attracted significant research interest due to their unique properties compared with conventional, macroscopic materials, for applications including solar cells, electronics, batteries, and sensors.<sup>1–11</sup> Recently, synthesis of nanomaterials with a range of sizes, structures, shapes, and chemical compositions has been an extremely important aspect of nanotechnology.<sup>12–15</sup> Synthesis of nanoparticles using

surfactants is an important area of research.<sup>15</sup> Surfactants provide solubility and control over nanoparticle growth and morphology during preparation, besides acting as stabilizers.<sup>14</sup> Cadmium sulfide (CdS) is an important group II–VI semiconductor material. CdS has a bandgap energy of 2.42 eV at room temperature and atmospheric pressure.<sup>16,17</sup> Owing to its wide bandgap, CdS is used as a window material for heterojunction solar cells to prevent recombination of photogenerated carriers, which improves solar cell efficiency.<sup>18</sup> CdS also has applications in light-emitting diodes,<sup>19</sup> nonlinear optics, heterogeneous photocatalysis, high-density magnetic information storage,<sup>20–22</sup> photodetectors,<sup>23</sup> and sensors,<sup>24</sup> as well as many

(Received March 15, 2015; accepted May 4, 2015;  
published online May 21, 2015)

other uses in the semiconductor industry. The properties of CdS nanoparticles are primarily driven by two factors: the increase in the surface-to-volume ratio, and drastic changes in the electronic structure of the material due to quantum-mechanical effects with decreasing particle size.<sup>25</sup> Moreover, CdS is known as one of the most promising photosensitive materials owing to its unique photochemical activities and strong visible-light absorption and emission.<sup>25</sup> Although much research has been carried out on CdS with various compositions and shapes,<sup>26</sup> preparation of CdS nanoparticles with good optical properties is still a very important area of research. In the present study, CdS nanoparticles capped with poly(ethylene glycol) (PEG), with controllable size and stability, were synthesized via chemical precipitation at room temperature. We investigated the effects of the molar ratios of the precursors cadmium chloride (CdCl<sub>2</sub>) and sodium sulfide (Na<sub>2</sub>S) on the size and morphological characteristics of the synthesized CdS nanoparticles using high-resolution transmission electron microscopy (HR-TEM) and x-ray powder diffraction (XRD) analysis. We also investigated the optical properties of synthesized CdS nanoparticles using ultraviolet-visible (UV-Vis) spectroscopy.

## EXPERIMENTAL PROCEDURES

### Synthesis of CdS Nanoparticles Capped with PEG

All chemicals employed were of analytical grade and used as received without further purification. Distilled water was used as solvent in all experiments. We adopted a simple chemical coprecipitation method to synthesize CdS nanoparticles of different sizes in colloidal solution using different molar aqueous solutions of CdCl<sub>2</sub> and Na<sub>2</sub>S as source materials and PEG as capping material. In this

procedure, CdCl<sub>2</sub> (0.1 M) and Na<sub>2</sub>S (0.1 M) were dissolved in 700 ml and 750 ml distilled water, respectively. The two solutions were stirred continuously for 30 min. PEG solution (5 wt.%) was stirred to achieve complete dissolution at room temperature. For synthesized sample S1 with Cd<sup>2+</sup>:S<sup>2-</sup> molar ratio of 1:0.5, 50 ml Na<sub>2</sub>S was added dropwise to 100 ml CdCl<sub>2</sub> under magnetic stirring. Then, 70 ml PEG surfactant was added to the reaction medium. White CdS nanoparticles precipitated and grew slowly in the solution according to the reaction



The precipitate was filtered and dried at 40°C for 36 h to remove any organic residues, water, and other byproducts formed during the reaction process. After sufficient drying, the precipitate was crushed into fine powder using a mortar and pestle. To study the effects of molar ratio on the size and optical properties of the CdS nanoparticles, samples with different Cd<sup>2+</sup>:S<sup>2-</sup> molar ratios were prepared as follows: S2 (1:0.63), S3 (1:1), S4 (1:2), and S5 (1:4).

### Instruments

XRD measurements were carried out using an X'Pert PRO (PANalytical, The Netherlands) with Cu K<sub>α</sub> radiation ( $\lambda = 0.15406$  nm). The x-ray generator was set to an acceleration voltage of 40 kV and a filament emission of 40 mA. The spectra were collected over a wide angle range ( $10^\circ < 2\theta < 80^\circ$ ). Specimens for TEM observation were prepared by dispersing CdS powder in distilled water and dropping it onto holey carbon grids. We observed the particle morphology and pore structure in detail using a HR-TEM (JEOL JEM-2010) operating at 200 kV. The images were digitally recorded using a charge-coupled device (CCD) camera (Keen View). UV-Vis spectra were measured over the range of

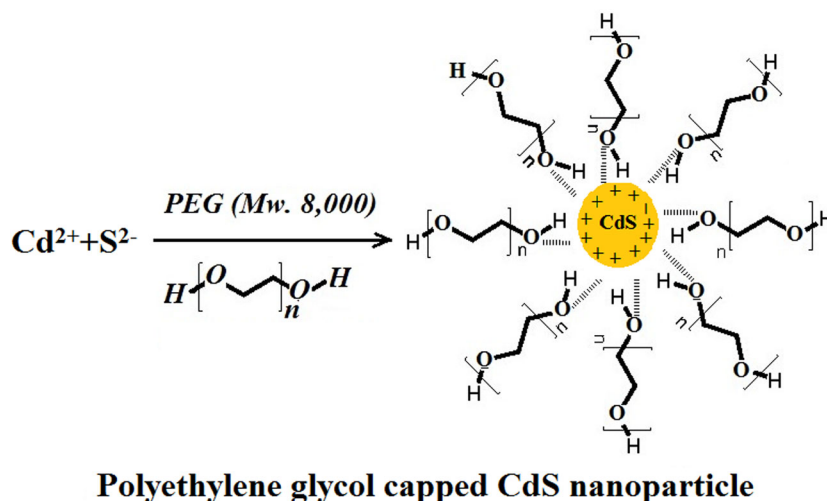


Fig. 1. PEG-capped CdS nanoparticles.

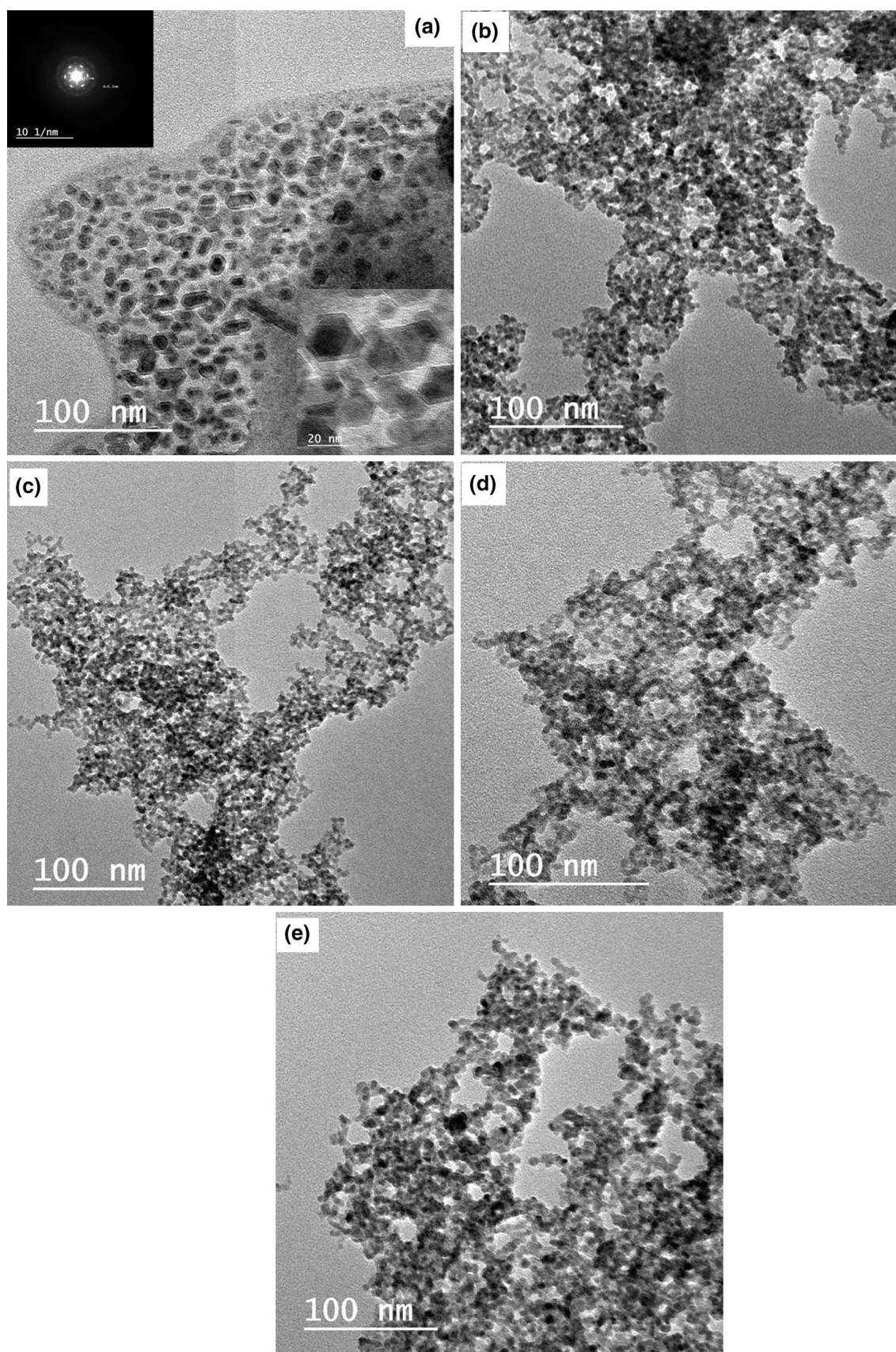


Fig. 2. HR-TEM images of CdS nanoparticles prepared with various  $\text{Cd}^{2+}:\text{S}^{2-}$  molar ratios and capped with PEG: (a) (1:0.5), (b) (1:0.63), (c) (1:1), (d) (1:2), and (e) (1:4). The inset in panel S1 shows the SAED pattern and the formation of lattice fringes, (a–e) corresponding to samples S1, S2, S3, S4, and S5 respectively.

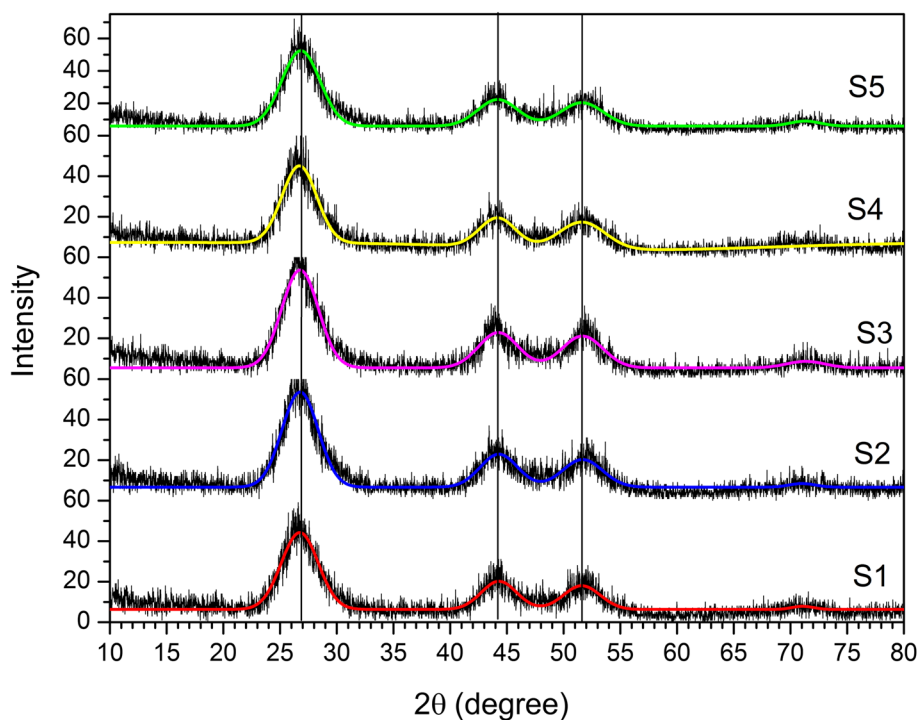


Fig. 3. XRD patterns and Gaussian fitting for CdS nanoparticles prepared with various  $\text{Cd}^{2+}:\text{S}^{2-}$  molar ratios and capped with PEG: S1 (1:0.5), S2 (1:0.63), S3 (1:1), S4 (1:2), and S5 (1:4).

**Table I. Optical bandgap, blue-shift, and particle size of CdS nanoparticles prepared with different molar ratios of  $\text{Na}_2\text{S}$  to  $\text{CdCl}_2$  plus PEG**

Sample	$\text{CdCl}_2:\text{Na}_2\text{S}$ Molar Ratio	Wavelength of Absorption Peak (nm)	Wavelength of Blue-shift (nm)	Energy Gap (eV)	Particle Size (nm) Estimated From:	
					XRD	UV
CdS (S1)	1:0.50	475	630	2.61	3.11	2.85
CdS (S2)	1:0.63	437	595	2.84	3.09	3.17
CdS (S3)	1:1	430	575	2.88	3.07	3.11
CdS (S4)	1:2	412	560	3.01	2.93	2.98
CdS (S5)	1:4	400	540	3.10	2.73	2.89

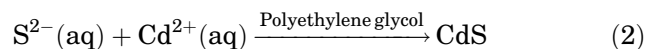
200 nm to 1000 nm using a spectrophotometer (Thermo Scientific Evolution 220). The samples were prepared as suspensions using distilled water. Fourier-transform infrared (FTIR) transmittance spectra of the prepared samples were measured using an FTIR spectrometer (JASCO 6100) in the mid-IR range by the KBr method.

## RESULTS AND DISCUSSION

### Formation of CdS Nanoparticles Capped with PEG

In preparatory experiments to investigate the assembly of CdS nanoparticles, PEG molecules were

attached simultaneously with CdS nanoparticles and the molar ratios of  $\text{CdCl}_2$  and  $\text{Na}_2\text{S}$  played an important role in the formation of the CdS nanoparticles. The ionic reaction can be expressed as



PEG is a typical polymer that can bind to CdS nanoparticles through its chelating oxygen and is used as a stabilizing agent. The synthesis of CdS nanoparticles capped with PEG is shown schematically in Fig. 1. According to this figure, the hydroxyl groups of PEG can cover the surface of the CdS nanoparticles



owing to the presence of van der Waals forces between the negatively charged oxygen groups in the molecular structure of PEG and the positively charged groups that surround the surfaces of the inert CdS nanoparticles.

### High-Resolution Transmission Electron Microscopy Measurements

TEM was employed to obtain direct information about the particle size, size distribution, morphology, and structure of the colloidal CdS prepared in aqueous solution by chemical precipitation with different molar ratios of the precursors. Figure 2 shows HR-TEM images of samples S1 to S5. It can be seen that the nanoparticles were distinguishable and that the particles were nearly small spheres and were not aggregated into large structures. These facts derive from the stabilizing polymer shell. However, some particles were in contact with each other and irregularities were accordingly observed. The agglomeration of particles may be due to their small dimensions and high surface energies. The samples were loosely distributed on the grid (note that significant uncertainties exist in the measurement of particle size by HR-TEM due to fuzzy particle boundaries). Even so, we measured that the average diameter changed from 2.5 nm to 4.5 nm for the five different preparation procedures discussed in "Experimental Procedures" section.<sup>27</sup> The selected-area diffraction (SAED) pattern in the inset to Fig. 2 for sample S1 consists of a central hole with broad concentric rings around it and exhibits a multicrystalline structure and diffraction rings corresponding to the cubic structure of CdS. The (111), (220), and (311) reflection planes can be observed in the SAED pattern of the CdS nanocrystals.<sup>28</sup> These results are typical of a very fine-grained material and indicate the crystalline nature of the as-synthesized samples. These results suggest that the PEG branches acted as a very effective stabilizer for preparation of a stable colloidal solution consisting of well-dispersed, monodispersed CdS nanocrystals.

### XRD Measurements

Figure 3 shows the XRD patterns for the prepared samples S1 to S5. The XRD patterns exhibit three remarkable peaks at  $2\theta$  values of  $26.55^\circ$ ,  $44.05^\circ$ , and  $52.17^\circ$ , which can be assigned to the (111), (220), and (311) Miller indices. CdS exists as two different minerals in nature, i.e., greenockite and hawleyite.<sup>29–31</sup> The hexagonal greenockite-forming wurtzite structure and the cubic hawleyite forming a zincblende structure. The hexagonal phase of CdS has two main peaks at  $2\theta$  of about  $28.3^\circ$  for the (101) plane and  $48.1^\circ$  for the (103) plane; the cubic phase has three main peaks at  $2\theta$  of about  $26.5^\circ$  for the (111) plane,  $43.9^\circ$  for the (220) plane, and  $51.9^\circ$  for the (311) plane.<sup>16,29</sup> From these

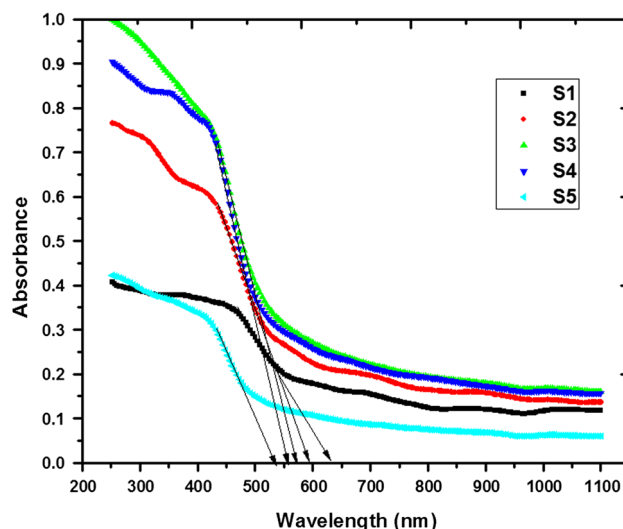


Fig. 4. UV-Vis absorption spectra of CdS nanoparticles prepared with different  $\text{Cd}^{2+}:\text{S}^{2-}$  molar ratios and capped with PEG: S1 (1:0.5), S2 (1:0.63), S3 (1:1), S4 (1:2), and S5 (1:4).

results, the Bragg reflections shown in the diffraction pattern of our samples correspond to a cubic structure with lattice constant of 5.81 Å. These data are in agreement with the standard reference [Joint Committee on Powder Diffraction Standards (JCPDS) 03-065-2887]. The XRD peaks were found to be very broad and considerably diffuse, indicating the very fine grain sizes of the samples.<sup>32</sup> Nanoparticles have a small number of crystal planes. This fact causes the lines in their diffraction pattern to become broader. This broadening in turn causes a loss of intensity in the signal of their diffraction patterns. On the other hand, bulk materials have sharp, narrow, high-intensity peaks. The broadness increases as well when a capping agent is used, which decreases the particle size.<sup>33</sup> Due to this broadening, the peak position and resolution were determined using the Gaussian peak fitting method, then the mean particle diameters were calculated. The average grain size of the samples was determined from the full-width at half-maximum (FWHM) of the most intense peak using Scherrer's formula [ $D = (0.94\lambda)/(\beta \cos \theta)$ ], where  $\lambda$  is the x-ray radiation wavelength,  $\beta$  is the FWHM of the XRD peak in radians, and  $\theta$  is the diffraction angle<sup>32</sup>. The particle sizes are listed in Table I. It can be seen that the particle size decreased with increasing  $\text{S}^{2-}$  concentration owing to the electronic configuration of  $\text{S}^{2-}$  ( $3p4$ ), because its tendency to interact with PEG and oxygen anions is greater than that of  $\text{Cd}^{2+}$ .

### UV-Vis

The absorption spectra of CdS nanoparticles prepared with various molar ratios of  $\text{CdCl}_2$  to  $\text{Na}_2\text{S}$  are shown in Fig. 4. The spectra exhibit well-defined different absorption peaks at 475 nm, 437 nm,

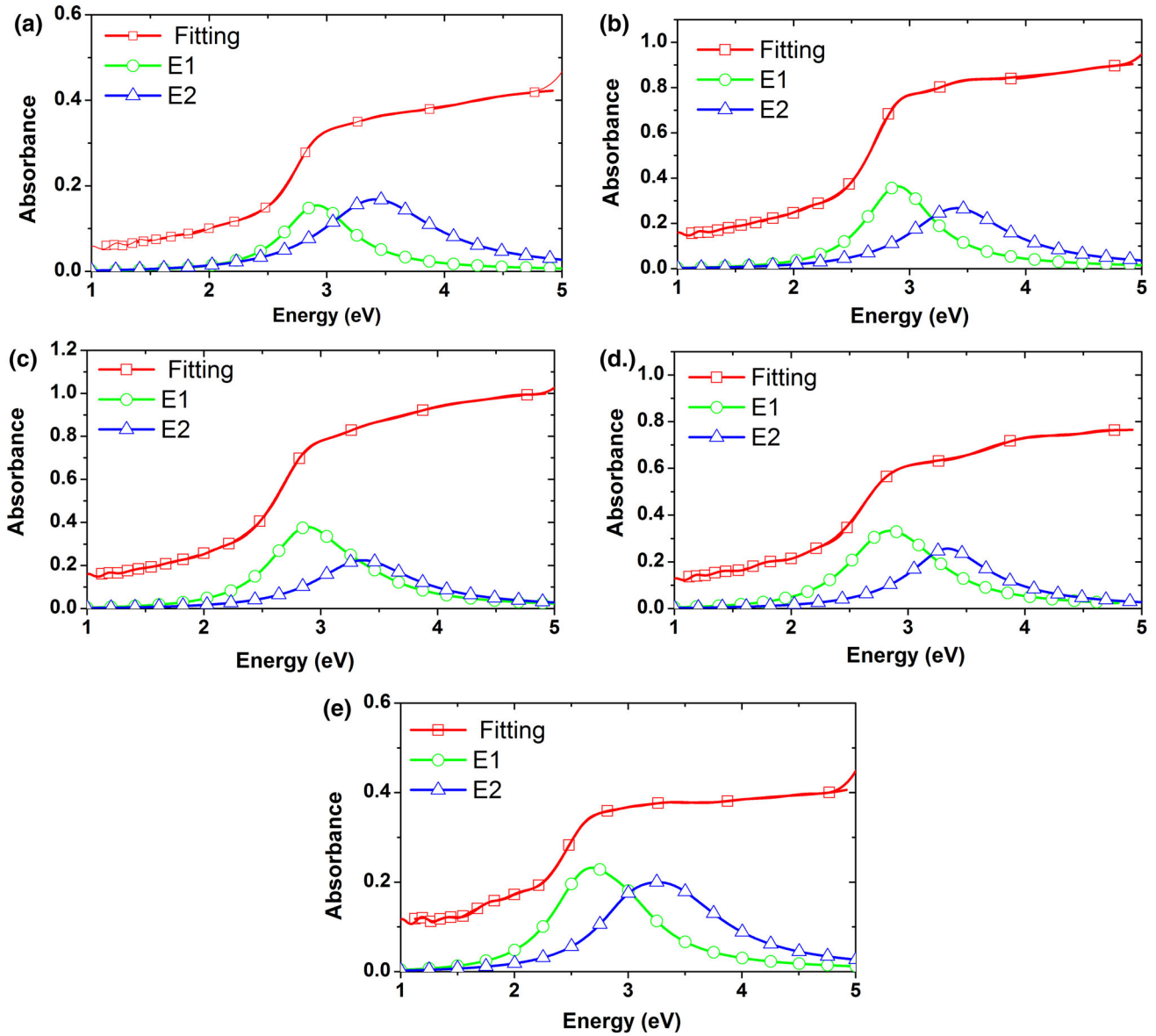


Fig. 5. Lorentz function fit and fit components for CdS nanoparticles prepared using different  $\text{Cd}^{2+}:\text{S}^{2-}$  molar ratios and capped with PEG: (a) (1:0.5), (b) (1:0.63), (c) (1:1), (d) (1:2), and (e) (1:4), (a–e) corresponding to samples S1, S2, S3, S4, and S5 respectively.

430 nm, 412 nm, and 400 nm for samples S1 to S5, respectively. The synthesized nanoparticles show a shift toward shorter wavelength in the optical absorption peak position compared with the bulk value (e.g., 2.4 eV for bulk at room temperature) due to the quantum confinement effect. The yellow color of these solutions indicates the formation of CdS nanoparticles. These results agree with the results of Shumbula et al.<sup>6</sup> In bulk CdS, an electron–hole pair is typically bound within a characteristic length called the Bohr exciton radius. As the particle size decreases, the electron and hole are constrained further, creating quantum confinement.<sup>34,35</sup> As a result of this confinement, the bandgap of the CdS nanoparticles increases, causing a blue-shift in the UV–Vis absorption spectra. The peaks associated with the CdS nanoparticles are assigned to the

optical transition of the first excitonic state ( $1s-1s$ ) transition band, i.e., to the valence band–conduction band transition. The exciton absorption peak decreases with particle size, owing to the quantum confinement of the electron–hole pairs. The particle size can be estimated from the experimental UV–Vis absorption spectrum using the following expression derived from the effective mass approximation (EMA)<sup>36,37</sup>:

$$\Delta E_g = E_g^{\text{nano}} - E_g^{\text{bulk}} = \frac{\hbar^2}{8r^2} \left( \frac{1}{m_e^*} + \frac{1}{m_h^*} \right) - \frac{1.8e^2}{4\pi\epsilon\epsilon_0 r} - \frac{0.124e^4}{\hbar^2(4\pi\epsilon\epsilon_0)^2} \left( \frac{1}{m_e^*} + \frac{1}{m_h^*} \right)^{-1}, \quad (3)$$

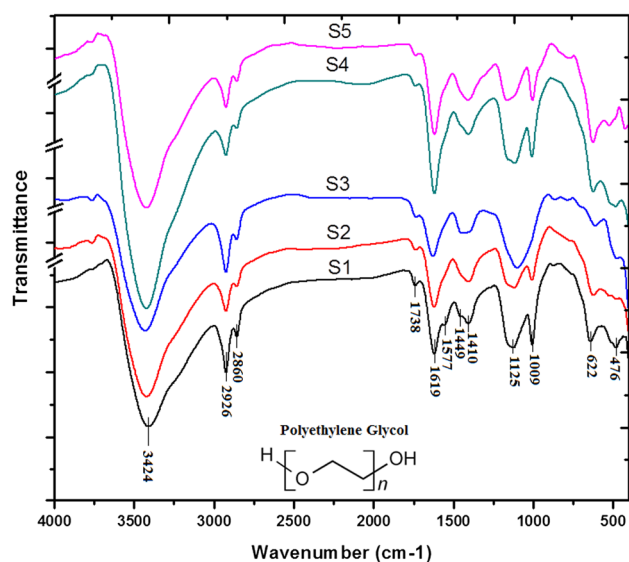


Fig. 6. FTIR spectra of CdS nanoparticles synthesized with various  $\text{Cd}^{2+}:\text{S}^{2-}$  molar ratios and capped with PEG: S1 (1:0.5), S2 (1:0.63), S3 (1:1), S4 (1:2), and S5 (1:4).

where  $E_g^{\text{nano}}$  is the bandgap energy of the nanoparticles as determined from the UV-Vis absorbance spectrum,  $E_g^{\text{bulk}}$  is the bandgap energy of bulk CdS at room temperature, which has a value of  $3.88 \times 10^{-19}$  J,  $h$  is Planck's constant,  $r$  is the particle radius (m),  $m_e^* = 0.19m_0$  is the effective mass of a conduction-band electron in CdS,  $m_h^* = 0.80m_0$  is the effective mass of a valence-band hole in CdS,  $e$  is the electron charge,  $\epsilon_0$  is the permittivity of free space, and  $\epsilon = 5.7$  is the high-frequency dielectric constant of CdS. Estimating the particle size of the present CdS samples using a value of 2.4 eV for  $E_g$  yielded values of 2.85 nm, 3.17 nm, 3.11 nm, 2.98 nm, and 2.89 nm for samples S1 to S5, respectively (Table I). It is clear that the sizes that we calculated indicate that the optical bandgap increases with decreasing particle size. It turns out that the particle size values calculated from the x-ray data differ from the values calculated from the UV-Vis spectra. It has been shown by a number of experimental studies that Eq. 1 cannot be expected to be quantitatively correct for very small particles. This fact is because, for small particles, the eigenvalues of the lowest excited states are located in a region of the energy band that is no longer parabolic. The particle-size dependence that we estimated accounts for the experimental size determined from the XRD line width using Scherrer's equation. Also, the possible agglomeration of the CdS nanoparticles might have affected the visible absorption spectrum and thereby the particle size; this point remains to be investigated. On the other hand, the absorption spectra were fit using a Lorentz model to quantitatively obtain the energy of the band-to-band transitions, as shown in Fig. 5. According to this model, two different components ( $E_1$  and  $E_2$ ) of the transition are observed at 2.6 eV

and 3.4 eV. The absorption bands  $E_1$  and  $E_2$  are attributed to the  $1s-1p$  and  $1s-1s$  transitions of the CdS nanoparticles, respectively.<sup>38</sup> These two bands appeared at energies higher than the reported bandgap of bulk CdS (2.43 eV).<sup>38-40</sup> For the  $E_1$  transitions, the peak positions for CdS synthesized with Cd:S molar ratio of approximately 1:4 are obviously blue-shifted compared with CdS synthesized with Cd:S molar ratio of approximately 1:0.5. The amount of shift of the  $E_1$  transitions is 0.02 eV due to the quantum size effect, where the particle size decreases with increasing ratio of Cd salt. The electronic structures of CdS nanoparticles were theoretically investigated by Brus,<sup>36</sup> where a blue-shift of the electronic levels above the Fermi energy  $E_F$  for CdS nanoparticles was observed. According to the EMA calculation, it was suggested that the  $1s$  state of CdS shifts above  $E_F$  by about 0.2 eV as a function of the nanoparticle radius. On the other hand, a downshift of the electronic levels of the bulk CdS toward  $E_F$  occurs.<sup>36</sup> We performed HR-TEM, XRD, and UV-Vis spectroscopy measurements on PEG-capped CdS nanoparticles dispersed in distilled water that were synthesized using five different molar ratios of  $\text{CdCl}_2$  to  $\text{Na}_2\text{S}$ , characterized by different particle sizes.

## Results of FTIR Spectroscopy

We carried out FTIR investigations to identify the CdS nanoparticles prepared using different molar ratios of the precursors and capped with PEG. Figure 6 shows FTIR spectra in the range from  $400 \text{ cm}^{-1}$  to  $4000 \text{ cm}^{-1}$  for the CdS nanoparticles synthesized via chemical precipitation. Strong interactions of water with CdS are reflected by the broad and strong peaks at  $3424 \text{ cm}^{-1}$  and  $1619 \text{ cm}^{-1}$  due to O-H stretching and O-H bending modes, respectively.<sup>41</sup> The shoulder at  $3250 \text{ cm}^{-1}$  can be assigned to PEG's OH groups. The bands appearing at  $2860 \text{ cm}^{-1}$ ,  $1449 \text{ cm}^{-1}$ , and  $1410 \text{ cm}^{-1}$  correspond to C-H stretching and bending vibrations. The bands due to C-O stretching are merged in a very broad envelope centered at  $1125 \text{ cm}^{-1}$  and  $1009 \text{ cm}^{-1}$ . These two bands arise from C-O, C-O-C linkage stretching and C-O-H bending vibrations. The peak at  $1094 \text{ cm}^{-1}$  characterizes PEG; according to previous work conducted by Tunc et al. and Philip et al.,<sup>42-44</sup> this peak appears at  $1000 \text{ cm}^{-1}$ . The shift of this peak toward higher frequencies is attributed to binding of C-C-O and C-C-H groups with CdS nanoparticles. The broad peaks at  $476 \text{ cm}^{-1}$  and  $622 \text{ cm}^{-1}$  are attributed to CdS bonding with oxygen from the hydroxyl groups of PEG chains. Therefore, the FTIR spectra indicate the existence of van der Waals interactions between PEG chains and CdS nanoparticles. The IR study confirms that the -C-O and -OH groups of PEG can readily bind with CdS nanoparticles. The FTIR spectra of CdS samples prepared with different molar ratios of  $\text{CdCl}_2$  to

Na<sub>2</sub>S (samples S1 to S5) and capped with PEG are very similar, except for a negligible shift in the absorption peaks owing to the interactions between CdS and PEG.

## CONCLUSIONS

We synthesized CdS nanoparticles using the chemical precipitation method. We calculated the crystalline structure, particle size, and morphology using XRD analysis, UV–Vis absorption spectroscopy, and HR-TEM measurements. UV–Vis absorption spectra revealed a blue-shift indicating the quantum confinement of the synthesized nanoparticles. The XRD patterns of all samples corresponded to the cubic structure of the CdS nanoparticles. HR-TEM revealed that the particles were formed with a spherical shape with different sizes depending on the molar concentration ratio.

## REFERENCES

1. P. Knauth and J. Schoonman, *Nanocrystalline Metals and Oxides: Selected Properties and Applications* (New York: Kluwer Academic, 2002), p. P1.
2. B. Bhushan, *Handbook of Nanotechnology*, 3rd ed. (Berlin: Springer, 2010).
3. P.S. Nair, T. Radhakrishnan, N. Revaprasadu, G.A. Kolawole, and P. O'Brien, *Polyhedron* 22, 3129 (2003).
4. K.S. Haram, M.B. Quinn, and A.J. Bard, *J. Am. Chem. Soc.* 123, 8860 (2001).
5. H. Zhao, E.P. Douglas, B.S. Harrison, and K.S. Schanze, *Langmuir* 17, 8428 (2001).
6. P.M. Shumbula, M.J. Moloto, T.R. Tshikhudo, and M. Fernandes, *S. Afr. J. Sci.* 106, 1 (2010).
7. M. Achermann, M.A. Petruska, S. Kos, D.L. Smith, D.D. Koleske, and V.I. Klimov, *Nature* 429, 642 (2004).
8. P. Alivisatos, *Nat. Biotechnol.* 22, 47 (2004).
9. J. Dupont, G.S. Fonseca, A.P. Umpierre, P.F.P. Fichtner, and S.R. Teixeira, *J. Am. Chem. Soc.* 124, 4228 (2002).
10. P. Praus, O. Kozak, K. Koci, A. Panacek, and R. Dvorsky, *J. Colloid Interface Sci.* 360, 574 (2011).
11. B. Gao, Y.J. Kim, A.K. Chakraborty, and W.I. Lee, *Appl. Catal. B* 83, 202 (2008).
12. A. Ulman, *Chem. Rev.* 96, 153 (1996).
13. H. Tang, M. Yan, H. Zhang, M. Xia, and D. Yang, *Mater. Lett.* 59, 1024 (2005).
14. P. Kumar, D. Kukkar, A. Deep, S.C. Sharma, and L.M. Bharadwaj, *Adv. Mater. Lett.* 3, 471 (2012).
15. N. Ramamurthy, G.R. Kumar, and G. Murugadoss, *Nanosci. Nanotechnol.* 1, 12 (2011).
16. M.J. Pauer and S.S. Chaure, *Chalcogenide Lett.* 12, 689 (2009).
17. K. Rajeshwar, N.R. de Tacconi, and C.R. Chenthamarakshan, *Chem. Mater.* 13, 2765 (2001).
18. A.M. Acevedo, *Sol. Energy Mater. Sol. Cells* 90, 2213 (2006).
19. H. Murai, T. Abe, J. Matsuda, H. Sato, S. Chiba, and Y. Kashiwaba, *Appl. Surf. Sci.* 244, 351 (2005).
20. A. Mukherjee, B. Satpati, S.R. Bhattacharyya, R. Ghosh, and P. Mitra, *Physica E* 65, 51 (2015).
21. R.R. Prabhu and M.A. Khadar, *Pramana* 65, 801 (2005).
22. N. Tessler, V. Medvedev, M. Kazes, S. Kan, and U. Banin, *Science* 295, 1506 (2002).
23. Y. Wang, S. Ramanathan, Q. Fan, F. Yun, H. Morkoc, and S. Bandyopadhyay, *J. Nanosci. Nanotechnol.* 6, 2077 (2006).
24. A. Ponzoni, E. Comini, and G. Sberveglieri, *Appl. Phys. Lett.* 88, 203101 (2006).
25. L. Wang, Y.S. Liu, X. Jiang, D.H. Qin, and Y. Cao, *J. Phys. Chem.* 111, 9538 (2007).
26. Y. Jun, Y. Jung, and J. Cheon, *J. Am. Chem. Soc.* 124, 615 (2002).
27. L. Qi, H. Colfen, and M. Antonietti, *Nano Lett.* 1, 61 (2001).
28. R.S. Dhage, A.H. Colorado, and H.T. Hahn, *Mater. Res.* 16, 504 (2013).
29. A. Latkiwicz and W. Abinski, *Mineral. Pol.* 35, 23 (2004).
30. R.J. Traill and R.W. Boyle, *Am. Mineral.* 40, 555 (1955).
31. J.J. Tan, Y. Li, and G.F. Ji, *Acta Phys. Pol.* A120, 501 (2011).
32. R. Seoudi, M. Kamal, A.A. Shabaka, E.M. Abdelrazek, and W. Eisa, *Synth. Met.* 160, 479 (2010).
33. M. Pal, N.R. Mathews, P. Santiago, and X. Mathew, *J. Nanopart. Res.* 14, 1 (2012).
34. E. Roduner, *Chem. Soc. Rev.* 35, 583 (2006).
35. V.I. Klimov, *Annu. Rev. Phys. Chem.* 58, 635 (2007).
36. L.E. Brus, *J. Chem. Phys.* 80, 4403 (1984).
37. Y. Kayanuma, *Phys. Rev. B* 38, 9797 (1988).
38. T.R. Ravindran, A.K. Arora, B. Balamurugan, and B.R. Mehta, *Nanostruct. Mater.* 11, 603 (1999).
39. V. Singh and P. Chauhan, *J. Phys. Chem. Solids* 70, 1074 (2009).
40. V. Singh, P.K. Sharma, and P. Chauhan, *Mater. Charact.* 62, 43 (2011).
41. A.Q. Zhang, Q.Z. Tan, H.J. Li, L. Sui, D.J. Qian, and M. Chen, *J. Nanopart. Res.* 16, 2197 (2014).
42. S. Tunc and O. Duman, *Colloids Surf. A* 37, 93 (2008).
43. D. Philip, *Spectrochim. Acta A* 75, 1078 (2010).
44. D. Philip, *Spectrochim. Acta A* 73, 650 (2009).